Journal of Power Sources 196 (2011) 3921–3932

Contents lists available at ScienceDirect

Journal of Power Sources

journal homepage: www.elsevier.com/locate/jpowsour

Online estimation of internal resistance and open-circuit voltage of lithium-ion batteries in electric vehicles

Yi-Hsien Chiang*, Wu-Yang Sean, Jia-Cheng Ke

Mechanical and System Laboratories, Industrial Technology Research Institute, Taiwan

ARTICLE INFO

Article history:
Received 31 August 2010
Received in revised form 5 December 2010
Accepted 5 January 2011
Available online 14 January 2011

Keywords:
Internal resistance
Open-circuit voltage
State-of-charge
State-of-health
Adaptive control
Equivalent circuit model

ABSTRACT

State-of-charge (SoC) and state-of-health (SoH) define the amount of charge and rated capacity loss of a battery, respectively. In order to determine these two measures, open-circuit voltage (OCV) and internal resistance of the battery are indispensable parameters that are obtained with difficulty through direct measurement. The motivation of this study is to develop an online, simple, training-free, and easily implementable scheme that is capable of estimating such parameters, particularly for the lithium-ion battery in battery-powered vehicles. Based on an equivalent circuit model (ECM), the electrical performance of a battery can be formulated into state-space representation. Also, underdetermined model parameters can be arranged to appear linearly so that an adaptive control approach can be applied. An adaptation algorithm is developed by exploiting the Lyapunov-stability criteria. The OCV and internal resistance can be extracted exactly without limitations of a system input signal, such as persistent excitation (PE), enhancing the method applicability for vehicular power systems. In this study, both simulations and experiments are established to verify the capability and effectiveness of the proposed estimation scheme.

1. Introduction

Specific energy and power in addition to cycle life are primary concerns of batteries utilized in electric vehicles (EV). The lithium-ion battery is believed to be able to potentially meet these requirements in the future. Hence, several well-known types of lithium batteries, such as lithium iron phosphate, lithium polymer, and nano-phosphate lithium-ion cells, have been developed. In addition, their reliability and durability are very susceptible to operational and environmental conditions, particularly in EV applications. To achieve the required EV traction power and range, low-voltage lithium-ion cells are generally connected in series and in parallel to construct a dedicated battery pack. A battery management system (BMS), along with protective circuitry and a communication bus, is provided for management, monitoring, and diagnosis. Measurement of state-of-charge (SoC) is one of basic functions of the BMS, which indicates the remaining charge of the battery so that the driver can be reminded to charge the battery prior to its depletion. It is known that inaccurate SoC determination is likely to cause catastrophic situations such as overdischarge or overcharge. In addition, state-of-health (SoH), which defines the battery performance relative to its fresh condition, is used to predict its end-of-life and aging. In another application, SoH is a measure used to analyze the effectiveness of the battery when incorporated with other power sources, i.e., hybrid energy storage systems, in order to extend battery cycle life. Generally, the SoH function is uncommonly seen in existing BMS's. However, there is an increasing need to monitor the battery performance in EV applications so as to prevent instant breakdown while driving.

Several methods for SoC determination have been proposed since 1938 [1]. Such methods can be generally categorized as direct or indirect approaches. One of the direct approaches simply indicates the remaining capacity by using online current integration [2]. Some studies have improved the previous-demonstrated accuracy by compensating for temperature and aging effects [3,4]. On the other hand, the indirect methods determine the SoC by using the battery's intrinsic relationship between the SoC and some electrical parameters such as open-circuit voltage (OCV) and impedance. For instance, the battery OCV naturally declines proportionately with the energy expenditure and is widely used for SoC indication [5–7]. Relying on an impedance spectroscopy analysis, the SoC and SoH can be accurately determined [8,9]. In recent years, the concept of adaptive estimation based on neural networks [10,11] or Kalman filtering [12,13] has been proven to be effective in SoC- and SoH-determination problems.

The SoH indication of the battery has attracted growing attention in the last decade for automotive applications, e.g., EV or hybrid EV (HEV). Typically, the SoH can be estimated through battery usage history or performance parameters. The usage history might involve normal charge–discharge cycles and abusive experiences, e.g., instances in which the operational limits of voltage,

* Corresponding author at: Rm. 200, Bldg. 58, 195, Sec. 4, Chung Hsing Rd., Chutung, Hsinchu 31040, Taiwan. Tel.: +886 3 591 7756; fax: +886 3 582 0452.
E-mail address: acloud.c@gmail.com (Y.-H. Chiang).

0378-7753/$ – see front matter © 2011 Elsevier B.V. All rights reserved.
doi:10.1016/j.jpowsour.2011.01.005

current, and temperature were exceeded. A data fusion technique is utilized to integrate the aforementioned data for the estimation of the remainder of battery lifetime. On the other hand, the battery aging also induces the loss of useful capacity and increase of internal resistance. The rated capacity measurement must apply a full charge–discharge process that is time-intensive and only suitable for testing in a laboratory. Instead, the battery impedance can be either directly analyzed by a spectroscopic instrument or be estimated through the transient response. For instance, some prevailing methods have analyzed the battery voltage profile by detecting the drop depth in a discharge operation [14,15] or subjecting the battery to a specific load demand, such as that seen during engine cranking [16,17], in order to determine the SoH. Prior studies [9,18–20] have also demonstrated that the accuracy of the SoH determination can be enhanced though a more elaborated impedance analysis. By employing battery electrical models, the internal resistance regarded as the low frequency impedance can be estimated by exploiting a sliding-mode control technique [21], or an extended Kalman filter [12].

In fact, the applicability of the existing SoC or SoH determining methods could be confined to some specific types of batteries. For example, the internal resistance of lithium-ion battery is insensitive to SoC variation within the range that is safe for use. Yet, the Coulomb counting or OCV measurements have no such limitation. Technically, the OCV is generally measured when the internal thermal stability of the battery has been reached. To do this, the battery should be discharged to each SoC set-point and then rested for a long time prior to measurement. To enhance the efficiency of the OCV measurement, a statistical analysis based on the data obtained from a fast discharge–charge process in laboratory has been presented [22]. In practice, a complex spectroscopic analysis of battery impedance is unnecessary as long as the internal resistance can be estimated instead. Furthermore, a prior study has illustrated how to determine the capacity fade of battery by identifying parameterized curves of the internal resistance with respect to the different working cycles based on a simple equivalent circuit model (ECM) [19]. In summation, the OCV and internal resistance parameters allow for determination of the SoC and SoH, respectively.

In this study, a novel method for online estimating of lithium-ion battery OCV and internal resistance simultaneously is presented. This method is conceived under following requirements for EV application: (1) online estimation, (2) simple mathematical operation, (3) no need of a specific load pattern or system excitation, (4) no prior time-intensive training process, and (5) easy implementation. To this end, a model-based estimation scheme is developed using an adaptive control approach that is primarily utilized to design controllers for nonlinear or linear systems with uncertainties. According to a simple ECM, the dynamics of a lithium-ion battery is described in state-space formulation, and the estimated parameters of the system appear linearly, which enables utilization of adaptive control techniques. The persistent excitation (PE) required for assuring parameter convergence in an adaptive control system is shown to be relaxed so that the convergent time that is required can be reduced. The proposed estimation system is the enhancement of the previous work [23], which is concerned with a method of estimation for battery parameters.

2. Mathematical battery model

Several existing battery models for characterizing battery electrochemical behavior have been constructed by using mathematical approaches from either macroscopic or microscopic perspectives. For microscopic models, partial differential equations are entailed for modeling the electrochemical interaction between two electrodes and electrolytes in order to determine the battery's

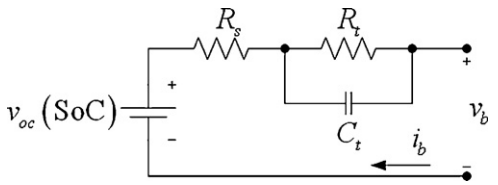

Fig. 1. A generalized ECM for lithium batteries.

effective capacity, current–voltage relationship, and heat generation [24,25]. However, such mathematical models are generally complex and need a numerical method to solve the problems, which are subject to initial and boundary conditions. On the other hand, the electrical models that regard the battery cell as a lumped system have been widely introduced to capture the dynamic characteristics in terms of current and voltage in order to ease the computation [26,27]. These have been demonstrated to agree with the dynamical response in discharge or charge operation within the order of 5% error, which is acceptable in terms of an engineering viewpoint. Due to the lower amount of required computation relative to the microscopic models, they are capable of determining the battery status online via the designed algorithm.

The electrical model described by a circuit that comprises the basic elements, such as resistor, inductor, and capacitor, is called an ECM. Those components are configured to properly match the measured impedance or transient response via system identification. Typically, the architecture of the circuit is composed of a fundamental ohmic resistor and one or more RC networks connected in series to simulate both the transient and steady responses of the battery. In order to capture the nonlinear characteristics of the battery, the resistance of each identified resistor is usually a nonlinear or piece-wise linear function with respect to SoC and temperature, depending on the types of batteries used. One of the ECMs used to simulate cell performance is illustrated in Fig. 1, where an ohmic resistor with resistance R_s, an RC network ($R_t//C_t$), and a DC source with voltage v_{oc} (OCV) that is function of SoC are connected in series. v_b is defined as the battery terminal voltage and i_b is the outflow current. It should be noted that, for simplicity, the above parameters are generally assumed to be independent of current direction. In other words, there is no hysteretic behavior being considered in Fig. 1. Accordingly, the impedance between the DC source and positive terminal can be given as

$$z(j\omega) = R_s + \frac{R_t}{jC_tR_t\omega + 1} \tag{1}$$

where ω is the frequency of i_b or v_b. The parameters in Eq. (1) can be identified through spectroscopic analysis, which is typically an approach applied in a laboratory. Alternatively, it is more straightforward to use battery voltage, current, and temperature such that an online estimation can be realized. To this end, the ECM is considered here for the development of an estimation algorithm. It is not only applicable to the scale of a cell, but also to that of a pack. For instance, a more precise ECM version with one resistor and three RC networks in series was utilized for modeling a battery pack to enhance battery modeling [28].

Using Kirchhoff's law, the dynamics of the ECM shown in Fig. 1 can be expressed as

$$\dot{v}_c = -\frac{1}{C_tR_t}v_c + \frac{1}{C_t}i_b \tag{2}$$

$$v_b = v_{oc} - R_si_b - v_c \tag{3}$$

where v_c is defined as the voltage across the RC network, as seen in Fig. 1, and cannot be determined because the voltage relating to R_s is unknown. It can be seen that Eqs. (2) and (3) are the state-space formulation, where v_c can be regarded as an estimated state

for an observer or Kalman filter design [12] as long as R_s, R_t, C_t, and v_{oc} are previously known. However, this is not the case because all the above parameters along with v_{oc} are still uncertain. In addition, more precisely, they should be variant with respect to SoC, temperature (T), and usage history (h), i.e.:

$$\mathbf{p} = \mathbf{p}(SoC, T, h), \qquad \mathbf{p}^T = \begin{bmatrix} R_s & R_t & C_t & v_{oc} \end{bmatrix} \tag{4}$$

where $\mathbf{p}$ is a parametric vector with the inclusion R_s, R_t, C_t, and v_{oc}. All of the battery parameters in (4) vary slightly within 90–10% of the SoC, implying that they can be estimated by any methodology that can account for such slowly varying behavior.

Because v_c is neither a measurable variable nor an estimated parameter following the above formulation, the removal of the v_c term from Eqs. (2) and (3) is desired in order to facilitate the algorithm derivation. To this end, one can differentiate v_b in Eq. (2) to yield:

$$\dot{v}_b = \dot{v}_{oc} - \dot{R}_s i_b - R_s \dot{i}_b - \dot{v}_c = \sigma(v_{oc})\chi - \sigma(R_s)\chi i_b - R_s \dot{i}_b - \dot{v}_c \tag{5}$$

where the differential operator $\sigma(A)$ and vector χ are defined as

$$\sigma(p) = \begin{bmatrix} \dfrac{\partial p}{\partial SoC} & \dfrac{\partial p}{\partial T} & \dfrac{\partial p}{\partial h} \end{bmatrix}, \qquad \chi^T = \begin{bmatrix} \dfrac{\partial SoC}{\partial t} & \dfrac{\partial T}{\partial t} & \dfrac{\partial h}{\partial t} \end{bmatrix}.$$

Here, p is any parameter in $\mathbf{p}$. It can be seen that the first two terms on the right-hand side of Eq. (5) are generated by deriving the higher-order dynamics of the battery in terms of the output voltage v_b. The complicated variation of a parameter is interpreted as multiplication of the change of the parameter with a state (SoC, T, or h), and the change of the state with time. In addition, Eq. (5) can be simplified with the following assumptions:

(A1) Small battery energy is consumed or regained relative to totally useful capacity. For example, a 40 Ah lithium-ion cell, the basic energy requirement for a city-EV, is assumed to conduct 1 C (40 A) discharge (generally less than this value at most time). The variation of SoC with respect to time is $\partial \mathrm{SoC}/\partial t = -40/(40 \times 3600) = -0.00028$, which is very small, i.e., $\partial \mathrm{SoC}/\partial t \approx 0$.

(A2) The cell temperature must be monitored and controlled at a predetermined level by a BMS in order to avoid a thermal runaway problem and keep thermal stress as low as possible for the longevity of the battery. Relying on the proper design of a cooling system/heater, the cell temperature rise/decrease should be slow. Hence, $\partial T/\partial t \approx 0$ holds for normal operating conditions.

(A3) Note that h represents a long term usage history such as the counts of working cycles or abuse. Thus, $\partial h/\partial t \approx 0$ definitely holds.

Accordingly, it follows that $\chi \approx 0$, thereby Eq. (5) can be rewritten as

$$\begin{aligned} \dot{v}_b &\approx -R_s \dot{i}_b - \dot{v}_c = -R_s \dot{i}_b + \frac{1}{C_t R_t} v_c - \frac{1}{C_t} i_b = -R_s \dot{i}_b - \frac{1}{C_t} i_b \\ &\quad + \frac{1}{C_t R_t}(v_{oc} - R_s i_b - v_b) \\ &= -\frac{1}{C_t R_t} v_b - R_s \dot{i}_b - \frac{R_t + R_s}{C_t R_t} i_b + \frac{v_{oc}}{C_t R_t} \end{aligned} \tag{6}$$

by substituting Eqs. (2) and (3) into Eq. (5). Obviously, the term v_c has been removed and a new variable $\dot{i}_b$ obtained. Yet, $\dot{i}_b$ can be easily computed by the differential of measured i_b.

3. Main results

3.1. Adaptive algorithm

According to Eq. (6), the dynamics of the battery is reinterpreted in terms of v_b. On the other hand, v_{oc}, $\dot{i}_b$, and i_b are regarded as the system inputs multiplied by the coefficients $1/C_t R_t$, R_s, and $(R_t + R_s)/C_t R_t$, respectively, to give new parameters to be determined. Because the parameters in Eq. (6) appear linearly, it is possible to employ an adaptive control approach that continuously updates uncertain parameters before the tracking error approaches zero. Recall that OCV is slowly varying within the battery's useable capacity. The region between 10% and 90% of SoC is generally unused in order to avoid the abusive conditions such as overcharge and overdischarge. Hence, OCV is considered as one of the parameters such that Eq. (6) can be written as

$$\dot{v}_b = \boldsymbol{\theta}^T \mathbf{X} \tag{7}$$

where

$$\boldsymbol{\theta}^T = \begin{bmatrix} \theta_1 & \theta_2 & \theta_3 & \theta_4 \end{bmatrix}^T = \begin{bmatrix} R_s & \dfrac{R_t + R_s}{C_t R_t} & \dfrac{1}{C_t R_t} & \dfrac{v_{oc}}{C_t R_t} \end{bmatrix},$$

$$\mathbf{X}^T = \begin{bmatrix} -\dot{i}_b & -i_b & -v_b & 1 \end{bmatrix}.$$

Note that v_{oc} and $1/C_t R_t$ are coupled together to become one new parameter. The estimated parameter vector in Eq. (7) is defined as

$$\hat{\boldsymbol{\theta}}^T = \begin{bmatrix} \hat{\theta}_1 & \hat{\theta}_2 & \hat{\theta}_3 & \hat{\theta}_4 \end{bmatrix}^T = \begin{bmatrix} \hat{R}_s & \widehat{\dfrac{R_t + R_s}{C_t R_t}} & \widehat{\dfrac{1}{C_t R_t}} & \widehat{\dfrac{v_{oc}}{C_t R_t}} \end{bmatrix}^T \tag{8}$$

The corresponding predicted state $\hat{v}_b$ is given as

$$\dot{\hat{v}}_b = \hat{\boldsymbol{\theta}}^T \hat{\mathbf{X}} + u \tag{9}$$

where

$$\hat{\mathbf{X}}^T = \begin{bmatrix} -\dot{i}_b & -i_b & -\hat{v}_b & 1 \end{bmatrix}$$

and u is input designed for regulation.

The design of an adaptive control system is to let a controlled state follow a reference signal. In our case, we expect that the tracking error of the predicted state can asymptotically tend towards zero, i.e.:

$$\lim_{t \to \infty} e = \lim_{t \to \infty} (v_b(t) - \hat{v}_b(t)) = 0. \tag{10}$$

It is known that Eq. (10) is also necessary for the convergence of the estimated parameters. By utilizing the technique used for the design of the adaptive controller [29], an adaptation law of the parameters can be developed.

Theorem. For a battery formulated in Eq. (7), its estimated dynamics is given by Eq. (9), and the condition expressed by Eq. (10) can be achieved by the adaptation law:

$$\dot{\hat{\boldsymbol{\theta}}} = \begin{bmatrix} \dot{\hat{\theta}}_1 \\ \dot{\hat{\theta}}_2 \\ \dot{\hat{\theta}}_3 \\ \dot{\hat{\theta}}_4 \end{bmatrix} = \begin{bmatrix} -g_1 \dot{i}_b e \\ -g_2 i_b e \\ -g_3 \hat{v}_b e \\ g_4 e \end{bmatrix} \tag{11}$$

together with the designed input:

$$u = \lambda e \tag{12}$$

where λ is positive semi-definite, i.e.:

$$\lambda \geq 0,$$

and the adaptation gains are positive definite:

$$g_i > 0, \quad i = 1, 2, 3, 4.$$

Proof. Invoking the Lyapunov-based design procedure, consider the Lyapunov function:

$$V(\tilde{v}_b, \tilde{\boldsymbol{\theta}}) = \frac{1}{2} e^2 + \frac{1}{2} \tilde{\boldsymbol{\theta}}^T \sum \tilde{\boldsymbol{\theta}} \tag{13}$$

where Σ is a positive definite matrix with proper dimensions. The estimated error vector $\tilde{\boldsymbol{\theta}}$ defined as the difference between actual and estimated parameters is

$$\tilde{\boldsymbol{\theta}}^T = \boldsymbol{\theta}^T - \hat{\boldsymbol{\theta}}^T = \begin{bmatrix} \tilde{\theta}_1 & \tilde{\theta}_2 & \tilde{\theta}_3 & \tilde{\theta}_4 \end{bmatrix}. \tag{14}$$

Note that V is a positive-definite function constituted by a quadratic polynomial in e and $\tilde{\theta}$. Hence, if V monotonically decreases, Eq. (10) is achieved. It is sufficed that its derivative shall be negative semidefinite. To this end, differentiating Eq. (13) along the trajectory of the system, it follows that

$$\begin{aligned}
\dot{V} &= \frac{\partial V}{\partial \tilde{v}_b}\frac{d\tilde{v}_b}{dt} + \frac{\partial V}{\partial \tilde{\theta}}\frac{d\tilde{\theta}}{dt} \\
&= \dot{e}e + \dot{\hat{\theta}}^T \sum \tilde{\theta} \\
&= (\dot{v}_b - \dot{\hat{v}}_b)e + (\dot{\theta}^T - \dot{\hat{\theta}}^T)\sum \tilde{\theta} \\
&= (\theta^T X - \hat{\theta}^T \hat{X} - u)e + (\dot{\theta}^T - \dot{\hat{\theta}}^T)\sum \tilde{\theta} \\
&= \left[-\tilde{\theta}_1 \dot{i}_b - \tilde{\theta}_2 i_b - (\tilde{\theta}_3 + \hat{\theta}_3)(e + \hat{v}_b) + \hat{\theta}_3 \hat{v}_b + \tilde{\theta}_4 - u\right] e \\
&\quad + (\dot{\theta}^T - \dot{\hat{\theta}}^T)\sum \tilde{\theta} \\
&= \left[-\tilde{\theta}_1 \dot{i}_b - \tilde{\theta}_2 i_b - \tilde{\theta}_3 \hat{v}_b + \tilde{\theta}_4 - \theta_3 e - u\right] e + (\dot{\theta}^T - \dot{\hat{\theta}}^T)\sum \tilde{\theta} \\
&= (\hat{X}^T e - \dot{\hat{\theta}}^T \sum)\tilde{\theta} - (\theta_3 e + u)e + \dot{\theta}^T \sum \tilde{\theta} \\
&= -(\theta_3 + \lambda)e^2 + \dot{\theta}^T \sum \tilde{\theta} \\
&\approx -\left(\frac{1}{\tau_t} + \lambda\right) e^2 \\
&\le 0
\end{aligned} \tag{15}$$

provided that

$$u = \lambda e, \quad \lambda \ge 0,$$

$$\dot{\hat{\boldsymbol{\theta}}} = \begin{bmatrix} \dot{\hat{\theta}}_1 \\ \dot{\hat{\theta}}_2 \\ \dot{\hat{\theta}}_3 \\ \dot{\hat{\theta}}_4 \end{bmatrix} = \sum^{-1} e\hat{\mathbf{X}} = \begin{bmatrix} -g_1 \dot{i}_b e \\ -g_2 i_b e \\ -g_3 \hat{v}_b e \\ g_4 e \end{bmatrix}$$

by letting $\sum = \mathrm{diag}((1/g_i) > 0, i = 1, 2, 3)$, and

$$\dot{\boldsymbol{\theta}} = \sigma(\theta)\chi \approx 0 \tag{16}$$

is used in accordance with (A1)–(A3). Here $\tau_t = C_t R_t$ is the polarization time-constant with regard to battery relaxation behavior. Particularly, the designed gain λ can be selected to be larger in order to dominate the convergent rate so as to shorten estimation time. By applying the LaSalle–Yoshizawa theorem [30] to Eq. (15), Eq. (10) follows.□

3.2. Convergence of parameters

Once $\hat{\boldsymbol{\theta}}$ converges to its actual value, each parameter can be evaluated via Eq. (8). It should be noted that Eq. (15) assures asymptotical stability of the state error e, rather than the estimated parametric error $\tilde{\boldsymbol{\theta}}$, as it is purposely cancelled to achieve sufficient system stability. As a general shortcoming of an adaptive control system, the PE is typically needed to assure the parameter stability where the PE is a type of design input needed to generate rich enough data for system identification [31]. Because the battery response is primarily determined by current command of the traction motor, the driving behavior may not produce a suitable current pattern to satisfy the PE. As a result, the estimated parameters may either take more time for convergence or become trapped at an incorrect equilibrium point. To evaluate the above problems, the stability condition of state error e should be analyzed as it appears in each term of the adaptation law (see Eq. (11)), i.e., the parameters stop updating as long as the state error approaches zero.

It can be found from Eq. (9) that $\hat{\theta}_1$, when coupled with $\dot{i}_b$, makes itself more sensitive to high dynamic operation, e.g., EV traction as well as regeneration, in comparison with the other parameters, implying that the convergent rate of $\hat{\theta}_1$ will be much faster than those of the other parameters. As a consequence, the condition:

$$\tilde{\theta}_1 \approx 0 \tag{17}$$

will be easily achieved in a short time. This phenomenon can be observed in tentative simulations in the following section.

According to Eqs. (10) and (17), we have

$$\begin{aligned}
\lim_{t\to\infty}(v_b(t) - \dot{\hat{v}}_b(t)) &= \lim_{t\to\infty}(\boldsymbol{\theta}^T \mathbf{X}(t) - \hat{\boldsymbol{\theta}}^T(t)\hat{\mathbf{X}}(t) - u(t)) \\
&= -\dot{i}_b(t)\lim_{t\to\infty}\tilde{\theta}_1(t) - i_b(t)\lim_{t\to\infty}\tilde{\theta}_2(t) \\
&\quad -\hat{v}_b(t)\lim_{t\to\infty}\tilde{\theta}_3(t) + \lim_{t\to\infty}\tilde{\theta}_4(t) - (\theta_3(t) \\
&\quad +\lambda)\lim_{t\to\infty} e(t) \\
&= -i_b(t)\lim_{t\to\infty}\tilde{\theta}_2(t) - \hat{v}_b(t)\lim_{t\to\infty}\tilde{\theta}_3(t) \\
&\quad +\lim_{t\to\infty}\tilde{\theta}_4(t).
\end{aligned} \tag{18}$$

Eq. (18) should equal to zero when the stability condition has been achieved, i.e.:

$$-i_b(t)\lim_{t\to\infty}\tilde{\theta}_2(t) - \hat{v}_b(t)\lim_{t\to\infty}\tilde{\theta}_3(t) + \lim_{t\to\infty}\tilde{\theta}_4(t) = 0. \tag{19}$$

On the other hand, let Eq. (3) be multiplied by $1/C_t R_t$ on both sides such that

$$\frac{v_b}{R_t C_t} = \frac{v_{oc}}{R_t C_t} - \frac{R_s}{R_t C_t} i_b - \frac{1}{R_t C_t} v_c \approx \frac{v_{oc}}{R_t C_t} - \frac{R_s + R_t}{R_t C_t} i_b. \tag{20}$$

Consider a situation where the RC network in the ECM has a low time-constant ($\tau_t = R_t C_t$) such that it acts like a pure resistor, i.e.:

$$v_c \approx R_t i_b \tag{21}$$

so as to make it possible to rewrite Eq. (20) as

$$-\theta_2 i_b - \theta_3 v_b + \theta_4 \approx 0. \tag{22}$$

Multiplying Eq. (22) by the constant $\alpha - 1$ and then adding it to Eq. (18) yields:

$$\begin{aligned}
&-i_b(t)\lim_{t\to\infty}(\alpha\theta_2 - \hat{\theta}_2(t)) - v_b(t)\lim_{t\to\infty}(\alpha\theta_3 - \hat{\theta}_3(t)) \\
&\quad + \lim_{t\to\infty}(\alpha\theta_4 - \hat{\theta}_4(t)) \approx 0.
\end{aligned} \tag{23}$$

It is illustrated that the adaptation algorithm achieves Eq. (10) and forces all estimated parameters to approach the values in proportion to their actual values scaled by an unknown constant α, i.e.:

$$\lim_{t\to\infty}\hat{\theta}_i(t) = \alpha\theta_i, \quad i = 2, 3, 4, \tag{24}$$

which is caused somehow by initial condition, driving pattern, and adaptation gain design. Unfortunately, this is the case in both simulations and experiments, as will be illustrated in a later section. Although actual values of the model parameter set are difficult to obtain in a straightforward manner, it is possible to evaluate all battery parameters other than the capacitance C_t. To see this, by using Eqs. (17), (20) and (24) we have

$$\begin{bmatrix} \hat{R}_s(t) \\ \hat{R}_t(t) \\ \hat{v}_{oc}(t) \end{bmatrix} = \begin{bmatrix} \hat{\theta}_1(t) \\ \dfrac{\hat{\theta}_2(t)}{\hat{\theta}_3(t)} - \hat{\theta}_1(t) \\ \dfrac{\hat{\theta}_4(t)}{\hat{\theta}_3(t)} \end{bmatrix} \tag{25}$$

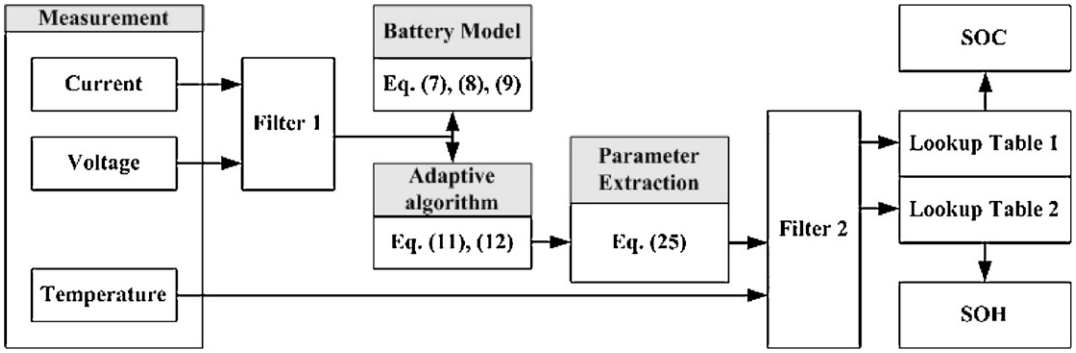

Fig. 2. Scheme of SoC and SoH determination based on adaptive control approach.

where $\left[\hat{R}_s \quad \hat{R}_t\right]^T$ and $\hat{v}_{oc}$ can be used to determine SoH and SoC, respectively.

3.3. Implementation of SoC and SoH determination

The proposed estimation method provides online monitoring of the battery's internal resistance and OCV for the determination of SoH and SoC, respectively. During the estimation procedure, a front-end process acquires current, voltage, and temperature via direct measurements. These signals or data may contain measuring noise such that a filtering process might be necessary to improve the estimation reliability. Later, the filtered data are sent to the developed estimation process for extracting battery internal resistance and OCV. The fact that the internal resistance gradually increases as the battery decays can be used to convert the estimated resistance data to a human-sense unit such as battery age or healthy ratio. On the other hand, the OCV curve, which decreases proportionately with the battery's usable energy, is used to determine the SoC. In addition, the battery's working temperature effects on the electrical characteristics shall be considered in the above SoC and SoH conversions. In order to reduce the estimation susceptibility to the measuring precision or disturbance, a filter with high bandwidth is introduced to process the estimated parameters prior to the conversion. A detailed scheme for the SoC and SoH determination is illustrated in Fig. 2. The relevant processes are summarized as follows.

1. *Measurement*: A BMS typically provides cell voltage and temperature monitoring by integrating dedicated measuring modules. Battery terminal voltage can be obtained by summing the cell voltages in series. A Hall-effect current sensor is deployed in the series loop for current management. Relying on the general BMS, the data requested for the estimation are acquired.
2. *Filter 1 and filter 2*: The bandwidth of the filter 1 shall be properly chosen to filter out only measurement noise without eliminating battery dynamics. However, the time constant of the filter 2 should be selected to be sufficiently large to enhance the robustness of the estimation against measuring disturbance. Also, the parameters of the filters are initially configured and held invariant.
3. *Battery model*: The ECM given by Eqs. (2) and (3) is reformulated into Eq. (7). It is assumed that Eq. (7) can catch dynamics of batteries used for EV applications and can be observed by Eq. (9) along with the estimated parameter vector Eq. (8).
4. *Adaptive algorithm*: The adaptation law given by Eqs. (11) and (12) is processed to update the estimated parameters.
5. *Parameter extraction*: The internal resistance and OCV are extracted via Eq. (25).
6. *SOC and SOH determination*: The lookup tables define data mappings between battery parameter and working status models in consideration with thermal effect. They are made through long-term tests in a laboratory or possibly provided by battery makers for such application.

4. Simulation and experimental results

The simulations and experiments are performed to validate the effectiveness of the proposed method on the estimation of battery internal resistance and OCV. Two simulations established in Simulink are used to verify the capability of determining the parameters in ECM accurately. The OCV is set to be fixed and slowly varying with respect to SoC in Simulations 1 and 2, respectively. Furthermore, two EV battery packs constructed from different types of lithium cells for a light EV [32] are utilized in two experiments to justify the applicability. To mimic a scenario in which the battery pack supplies motive power to the light EV running in an urban area, the American FTP-75 driving cycles are adopted to generate the demanded power pattern by means of ADVISOR, a vehicle simulator. Automated cell-test equipment commands the attached battery pack to discharge or charge following a power

Table 1
Battery parameters and adaptation gains.

Group	Symbol	Simulation 1	Simulation 2	Experiment 1	Experiment 2
Battery parameters	v_{oc} (V)	12.6	12.6[a]	70.7[a]	69.3[a]
	R_s (mΩ)	0.1	0.1	76.82[b]	10.22[b]
	R_t (mΩ)	0.05	0.05	–	–
	C_t (F)	5	5	–	–
Adaptation gains	λ	0.2	0.2	0.4	0.4
	g_1	0.001	0.001	0.001	0.0004
	g_2	0.005	0.005	0.5	0.5
	g_3	0.05	0.05	0.8	0.8
	g_4	1	1	1	1

[a] The OCV is varying with the change of the capacity. The value shown here represents its initial state in simulation or experiments.
[b] The ohmic resistance is measured by an impedance measuring instrument as its actual value.

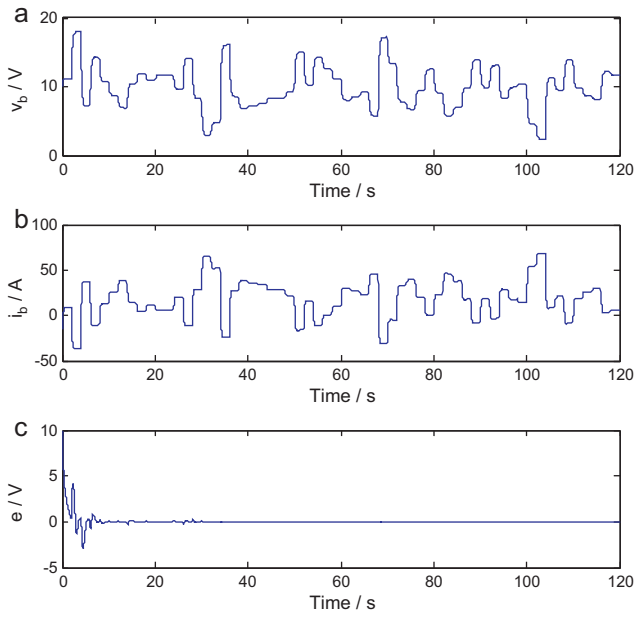

Fig. 3. Measurements and estimated state error in Simulation 1: (a) terminal battery voltage, (b) battery outflow current, and (c) estimated state error.

pattern in a laboratory. The voltage and current of the battery pack are measured via the equipment and recorded in its remote PC. Because the scheme works in an open-loop manner, the estimation process can be performed offline without loss of reality. To this end, the recorded data are loaded into the Simulink environment to simulate the real estimation condition. In the following simulations and experiments, the measured states are battery working voltage v_b and current i_b. The estimated battery voltage $\hat{v}_b$ is produced by the ECM with estimated model parameters $\hat{\theta}_i$, $i = 1\sim4$ as well as the measured current. The primary estimated state for SOC is OCV $\hat{v}_{oc}$, and the primary estimated parameters for SOH are internal resistance $\hat{R}_s$ and $\hat{R}_t$. $\hat{v}_{oc}$, $\hat{R}_s$, and $\hat{R}_t$ can be extracted from the model parameters. The system parameters required for the simulations and experiments are specified in Table 1.

4.1. Simulation 1

The objective of this simulation is to verify the accuracy of the proposed method when estimating the internal resistance and OCV. A battery exactly described by Eqs. (2) and (3) is assumed to discharge and charge subject to a random load as depicted in Fig. 3(a). The load voltage is equal to the battery terminal voltage and determines the current profile as shown in Fig. 3(b), where the positive value denotes outflow current. The estimated parameters are initially set at $\hat{\theta}_1(0) = \hat{R}_s(0) = 0.2\,\Omega$, $\hat{\theta}_2(0) = \widehat{(R_t + R_s)/C_t R_t}(0) = 0.01\,\mathrm{F}^{-1}$, $\hat{\theta}_3(0) = \widehat{1/C_t R_t}(0) = 6\,\mathrm{s}^{-1}$, and $\hat{\theta}_4(0) = \widehat{v_{oc}/C_t R_t}(0) = 40\,\mathrm{V\,s}^{-1}$. The trajectory of the estimated error is depicted in Fig. 3(c) and converges to zero within 10 s. The estimated parameters and their actual values are depicted in Fig. 4, where the blue and black lines denote the actual and estimated values, respectively. It can be found that only $\hat{\theta}_1$ agrees with the actual value of 0.1 Ω, reflecting the observation made in Eq. (17), and the others stop updating after the convergence of the estimated error. The resulting internal resistance and OCV are depicted in Fig. 5 and both tend to their actual values within 40 s despite the accuracy and traces of the estimated parameters. This demonstrates the effectiveness of the proposed method when applied to the ECM along with the invariant parameters.

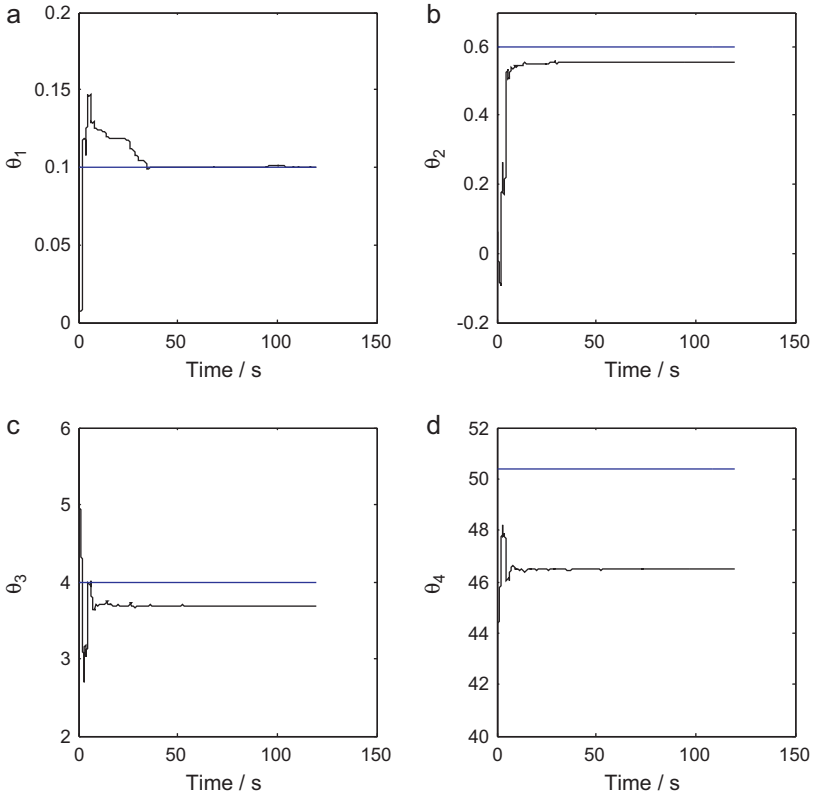

Fig. 4. Trajectories of estimated parameters in Simulation 1: (a) θ_1, (b) θ_2, (c) θ_3, and (d) θ_4; the blue and black lines denote actual and estimated values, respectively. (For interpretation of the references to color in this figure legend, the reader is referred to the web version of the article.)

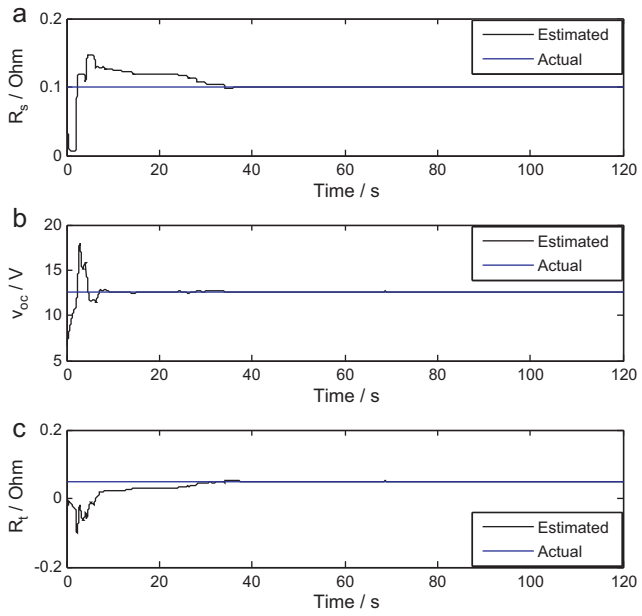

Fig. 5. Estimated internal resistance and OCV in Simulation 1: (a) R_s, (b) v_{oc}, and (c) R_t.

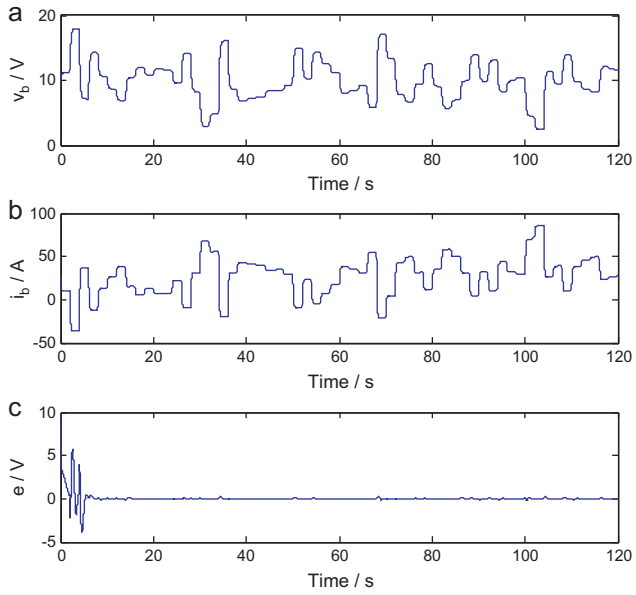

Fig. 6. Measurements and estimated state error in Simulation 2: (a) terminal battery voltage, (b) battery outflow current, and (c) estimated state error.

4.2. Simulation 2

A ECM where the OCV is monotonically varying throughout the entire operation is considered in this simulation. Other than the OCV, the parameters and their initial values are invariant, similar to the ones set in Simulation 1. A random load profile used to excite the system is also the same and is depicted in Fig. 6(a). Due to the rise of the OCV, the battery supplies more and regains less current during the discharge and charge operations, respectively, as depicted in Fig. 6(b) when comparison with Fig. 3(b). It can be observed from Fig. 6(c) that the estimated error converges to zero within 10 s. The estimated parameters are depicted individually in Fig. 7 for comparison to their actual values, and the following brief conclusions are drawn.

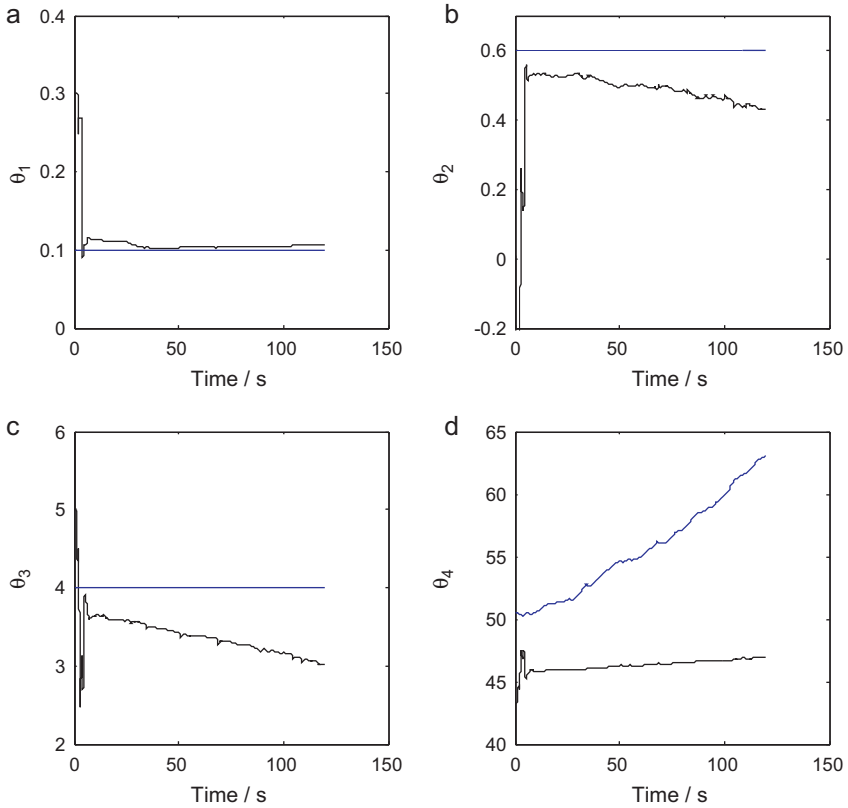

Fig. 7. Trajectories of estimated parameters in Simulation 2: (a) θ_1, (b) θ_2, (c) θ_3, and (d) θ_4; the blue and black lines denote actual and estimated values, respectively. (For interpretation of the references to color in this figure legend, the reader is referred to the web version of the article.)

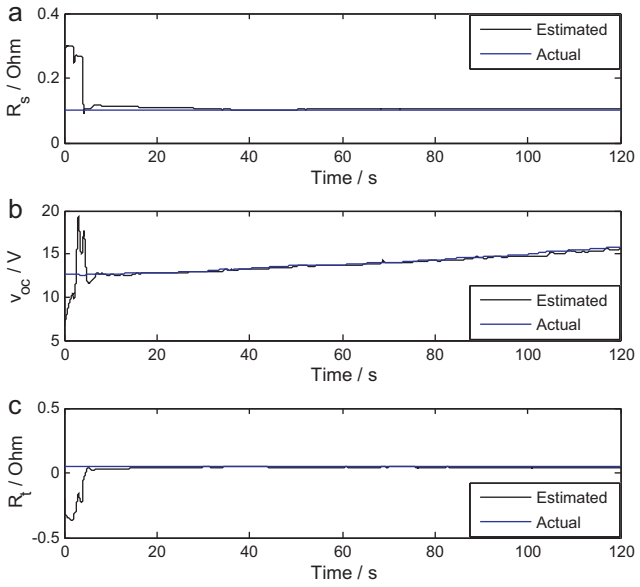

Fig. 8. Estimated internal resistance and OCV in Simulation 2: (a) R_s, (b) v_{oc}, and (c) R_t.

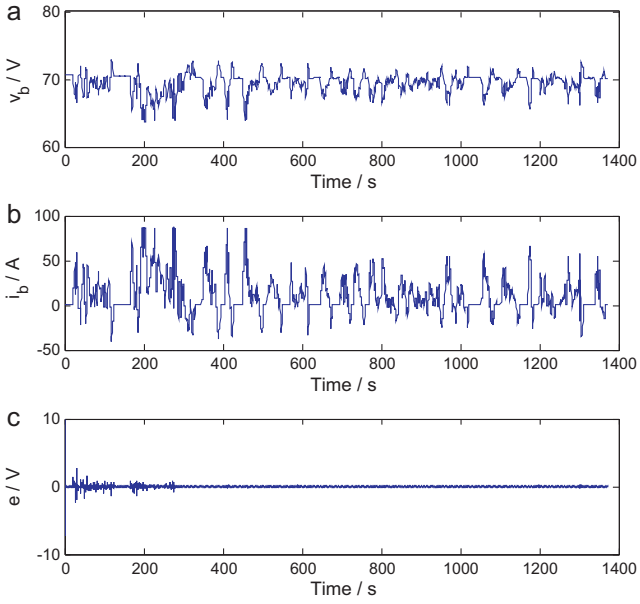

Fig. 9. Measurements and estimated state error in Experiment 1: (a) terminal battery voltage, (b) battery outflow current, and (c) estimated state error.

(i) The estimated ohmic resistance identical to $\hat{\theta}_1$ converges to its actual value as fast as the case in Simulation 1, as shown in Fig. 7(a). It is evident that the condition set forth in Eq. (17) is true in either two cases.

(ii) Comparatively, the other estimated parameters, $\hat{\theta}_2 \sim \hat{\theta}_4$, diverge from the actual profiles as illustrated in Fig. 7(b)–(d). However, the resulting internal resistance and OCV still tend to their actual values after 10 s as shown in Fig. 8(a)–(c). It can be inferred from Figs. 7 and 8 that the multiplier α is varying during the entire process, rather than being held constant as in Simulation 1.

Simulations 1 and 2 verify the proposed method based on the assumptions (A1)–(A3) and can accurately estimate the internal resistance and OCV of the battery that can be exactly modeled by Eqs. (2) and (3).

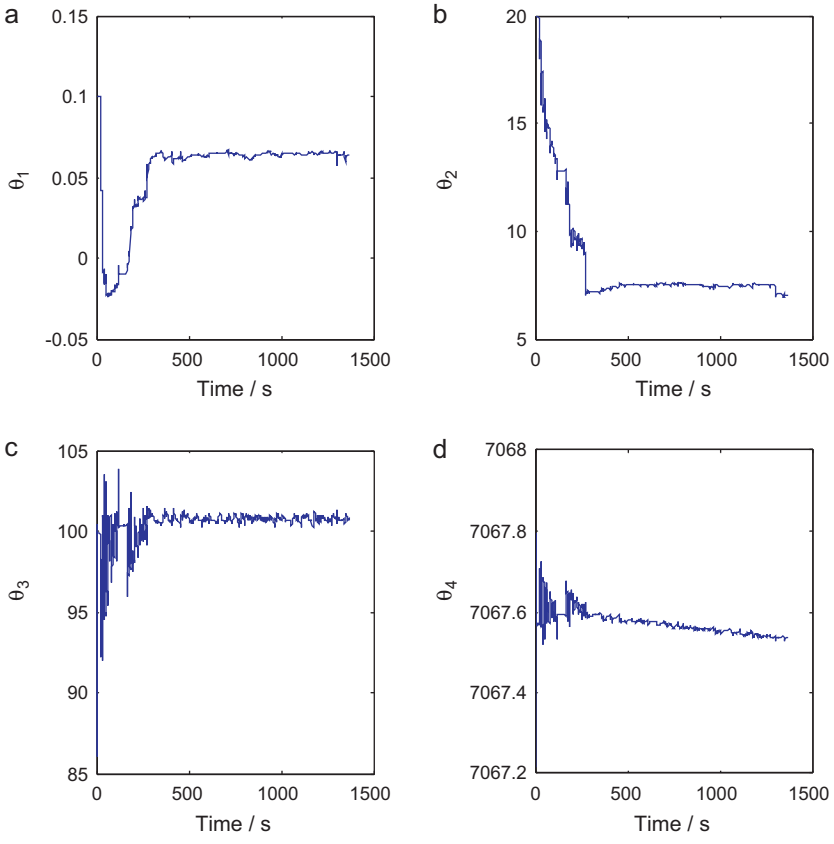

Fig. 10. Trajectories of estimated parameters in Experiment 1: (a) θ_1, (b) θ_2, (c) θ_3, and (d) θ_4.

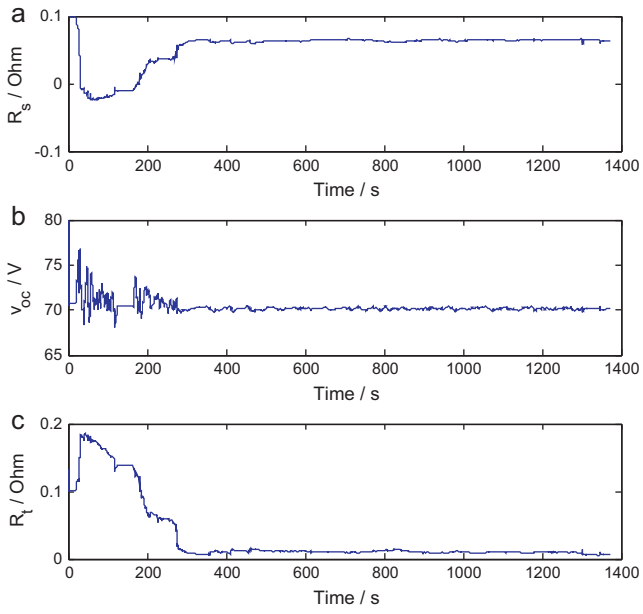

Fig. 11. Trajectories of estimated internal resistance and OCV in Experiment 1: (a) R_s, (b) v_{oc}, and (c) R_t.

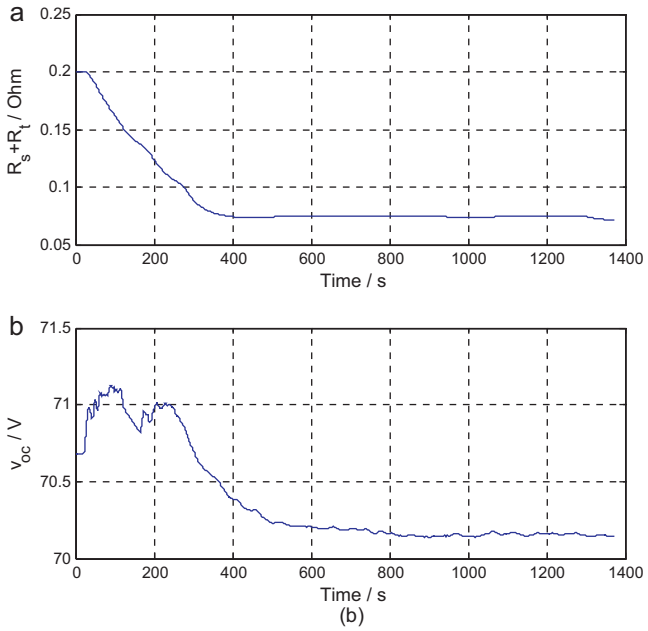

Fig. 12. Filtered estimated internal resistance and OCV in Experiment 1: (a) internal resistance and (b) OCV.

4.3. Experiment 1

Practically, the ECM employed here is simplified to reduce the order of model complexity and facilitate the development of the estimation algorithm. The accuracy affected by unmodeled dynamics should be investigated by using a real battery. To this end, lithium iron phosphate cells are connected in series to reach a nominal voltage of 70 V to fulfill the voltage requirement of a light EV. An experiment is established to let the automated cell-test machine manage the discharge and charge operation in accordance with the converted power pattern. Meanwhile, the ambient temperature of the battery pack is managed by an air conditioner to remove the accumulated heat within the cells during operating. Thus, the cells' temperatures would appear in slowly varying manner so as to meet the assumption (A2). Throughout one cycle of the FTP-75, the battery voltage and outflow current are depicted in Fig. 9(a) and (b), respectively. The voltage fluctuates between 73 and 64 V and the maximum discharge/charge current varies up to 95/40 A. The initial values for the estimated parameters are $\hat{\theta}_1(0) = 0.1\,\Omega$, $\hat{\theta}_2(0) = 20\,\mathrm{F}^{-1}$, $\hat{\theta}_3(0) = 100\,\mathrm{s}^{-1}$, and $\hat{\theta}_4(0) = 7067.2\,\mathrm{V\,s}^{-1}$. As illustrated in Fig. 9(c), the tracking error converges to zero after 5 min. With proper gain selection and prior knowledge of initial parametric values, faster convergence can be achieved. The trajectories of the estimated parameters are depicted in Fig. 10(a)–(d). As shown in Fig. 10(a)–(c), the parameters $\hat{\theta}_1$, $\hat{\theta}_2$, and $\hat{\theta}_3$ converge to steady values of 0.063, 7.5, and 100.5, respectively, with small fluctuations. Unlike the others, the parameter $\hat{\theta}_4$ follows a descending manifold, as illustrated in Fig. 10(d), as the OCV drops as a function of the decrease of battery stored energy.

The resulting internal resistance and OCV are depicted in Fig. 11. The ohmic resistance trajectory equals to the parameter $\hat{\theta}_1$, as shown in Fig. 11(a). The polarized resistance tends to 0.01 Ω and the OCV descends slowly from its initial value of 70.75 to 70.15 V at the end of the process. In order to enhance the reliability of SoC and SoH determination, the estimated internal resistance ($\hat{R}_s + \hat{R}_t$) and OCV are processed through the filter 2 to become smooth, as shown in Fig. 12. $\hat{R}_s + \hat{R}_t$, regarded as low frequency impedance that is approximated as 75 mΩ, is close to 76.82 mΩ, the value obtained via an impedance measuring instrument, as shown in Table 1. It is shown in Fig. 12(b) that the estimated OCV declines slowly in the process except for the first 5 min of the adaptation process. The accuracy analysis of the OCV estimation will be verified in the next experiment.

4.4. Experiment 2

A lithium polymer battery pack is constructed to reach a nominal voltage of 68 V and a higher energy density than the one used in the first experiment in order to investigate the compatibility of the proposed method with the different types of EV batteries. Again, the battery pack is managed to discharge and charge in accordance with the same power profile and thermal environment used in Experiment 1. The estimated parameters are initially set at $\hat{\theta}_1(0) = 0.05\,\Omega$, $\hat{\theta}_2(0) = 15\,\mathrm{F}^{-1}$, $\hat{\theta}_3(0) = 100\,\mathrm{s}^{-1}$, and $\hat{\theta}_4(0) = 6875\,\mathrm{V\,s}^{-1}$. The battery working voltage, current, and estimated error are depicted in Fig. 13. The voltage fluctuates between 70 and 65 V and its range is larger than that of the pervious battery pack due to their different electrochemical properties. The estimated error has been attenuated to near zero after 450 s. The estimated parameters depicted in Fig. 14 have trajectories similar to those in Simulation 2. It is noted in Fig. 14(a) and (b) that the parameters tripped off their steady values at the end of the process. As shown in Fig. 13, between 1,300 and 1,350 s, the voltage spikes and outflow current have the same side, which disagrees with the normal voltage–current behavior because the internal resistance would cause excess voltage drop/bounce on the discharge/charge operation. This fault might be caused by a measurement or data transmission error that can be regarded as a disturbance. The resulting ohmic resistance, OCV, and polarization resistance are plotted in Fig. 15(a)–(c), respectively. It can be shown that the disturbance affects the estimated internal resistance more than the OCV. $\hat{R}_s + \hat{R}_t$ and estimated OCV processed through the filter 2 are shown in Fig. 16. After 450 s, $\hat{R}_s + \hat{R}_t$ converges to a steady value of 20 mΩ, and the estimated OCV approaches a declined manifold. Also, the robustness of the proposed scheme is improved by examining the $\hat{R}_s + \hat{R}_t$ curve at approximately 1,320 s. In actuality, the internal resistance measured by the impedance measuring instrument is 10.22 mΩ, as shown in Table 1, and is close to the estimated ohmic resistance rather than low frequency impedance.

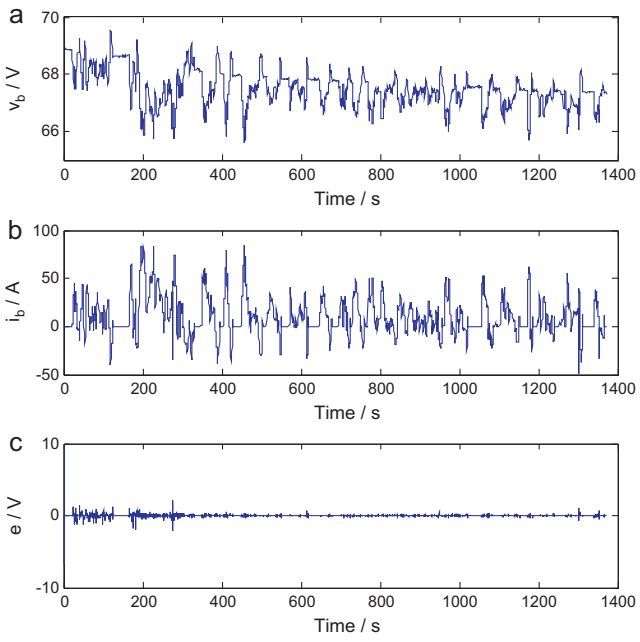

Fig. 13. Measurements and estimated state error in Experiment 2: (a) terminal battery voltage, (b) battery outflow current, and (c) estimated state error.

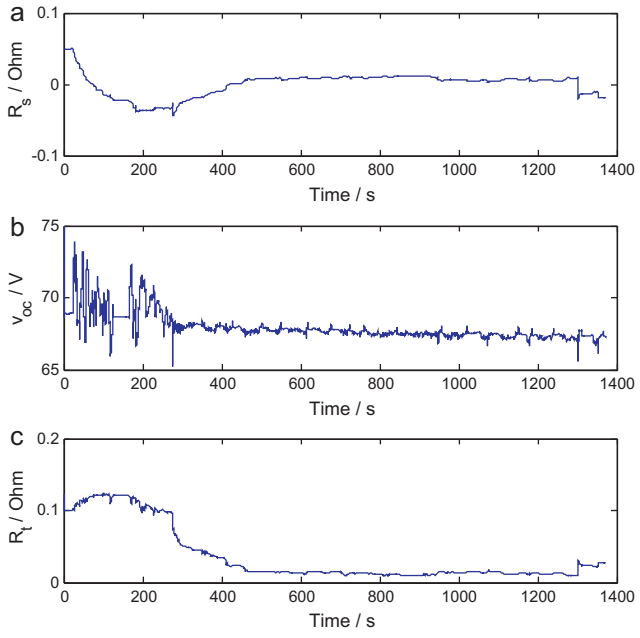

Fig. 15. Trajectories of estimated internal resistance and OCV in Experiment 2: (a) R_s, (b) v_{oc}, and (c) R_t.

For the comparison with actual OCV at the beginning of estimation process, the parameters are initially set to be equal to those obtained from the previous results, i.e., $\hat{\theta}_1(0) = 0.01\,\Omega$, $\hat{\theta}_2(0) = 2\,\mathrm{F}^{-1}$, $\hat{\theta}_3(0) = 100\,\mathrm{s}^{-1}$, and $\hat{\theta}_4(0) = 6882.6\,\mathrm{V\,s}^{-1}$. By reusing the battery voltage and current data, the estimated OCV with respect to depth of discharge (DoD) after the filtering process is depicted in Fig. 17. On the other hand, the actual OCV is measured after a process in which the battery pack is discharged with a low current of

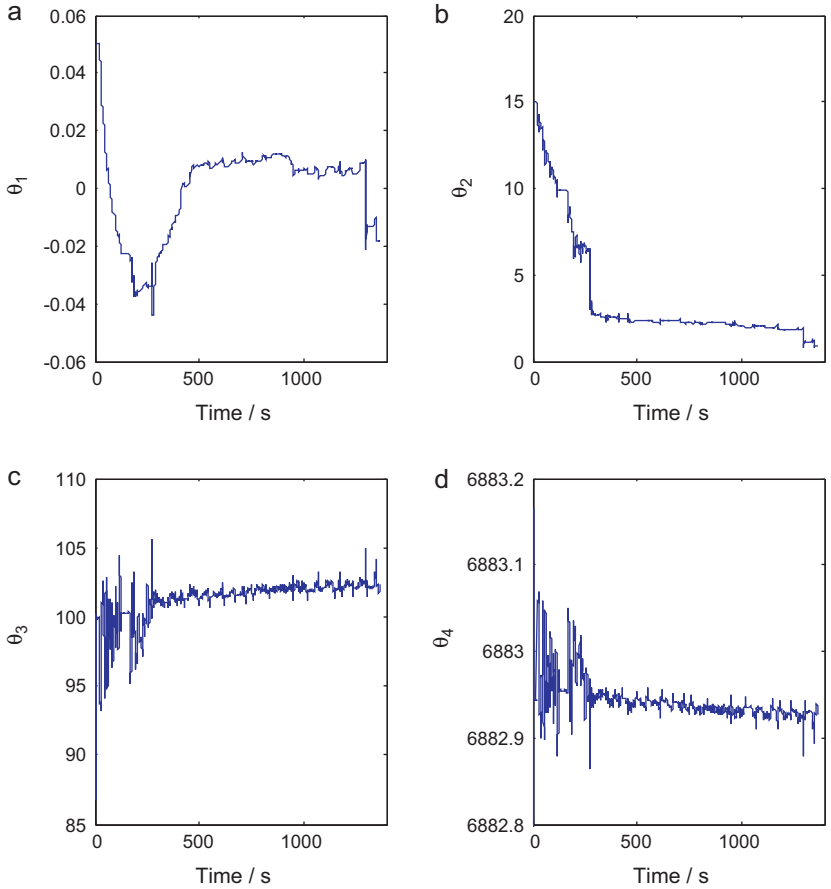

Fig. 14. Estimated parameters in Experiment 2: (a) θ_1, (b) θ_2, (c) θ_3, and (d) θ_4.

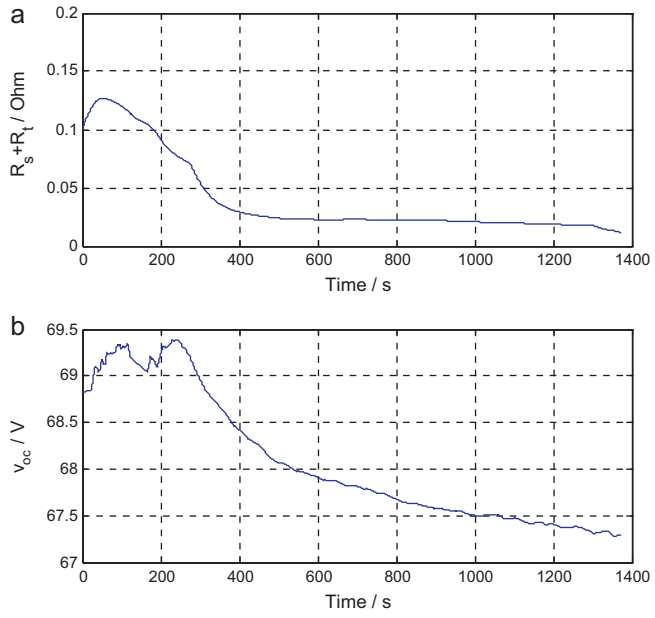

Fig. 16. Filtered estimated internal resistance and OCV in Experiment 2: (a) internal resistance and (b) OCV.

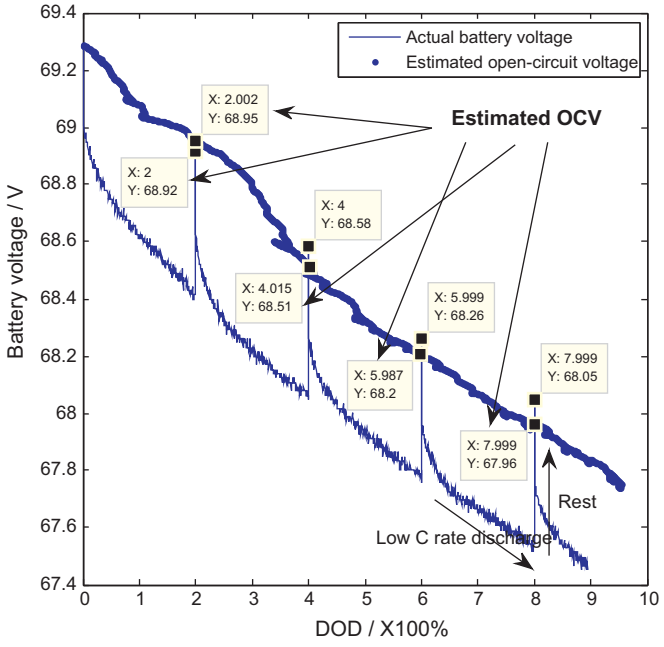

Fig. 17. Comparative results of estimated and actual OCV with respect to DOD.

5 A until the 2% DoD is met and then rested for 30 min. This process is repeated four times, and the measured voltage is plotted in Fig. 17 by a solid line. The actual OCV at the 2%, 4%, 6%, and 8% DoD are indicated in comparison with the estimated ones. It is found that the maximum estimated error is ±0.1 V in OCV or ±0.5% in DoD (or SoC). The overall estimated error for the lithium polymer batteries without considering thermal effect is about ±1% SoC at maximum, by adding maximum estimation discrepancy (±0.1 V OCV) at the same SoC (seeing the estimated OCV curve at 3.3% DoD in Fig. 17).

The capability of the proposed scheme, according to the simulation and experimental results are summarized as follows.

(i) For a battery exactly modeled by the ECM shown in Fig. 1, the proposed method can be performed online and can accurately estimate the internal resistance and OCV.
(ii) For an EV battery pack constructed by either lithium polymer or lithium iron phosphate type of cells, the proposed scheme can be performed online and can reliably estimate the ohmic resistance, polarized resistance, and OCV with a small error so as to determine the SoC and SoH.
(iii) The proposed scheme is robust to the disturbance caused by measuring or data transmission error.

5. Conclusions

In this study we proposed a technique for identifying battery internal resistance and OCV regarding SoH and SoC determination, respectively. Based on an ECM simply composed of one resistor and one RC network connected in series to capture the essential dynamics of a lithium-ion battery, an online estimation method of the model parameters is developed by using an adaptive control approach that has been widely applied to nonlinear control systems with parameter uncertainties. The adaptation law is devised to assure that estimated state error asymptotically decreases to zero by invoking the Lyapunov stability criteria. It is demonstrated that the internal resistance and OCV can be accurately extracted from the estimated parameters once the estimated state error tends to zero. Hence, the PE condition demanded to assure the asymptotical stability of the parameters in the adaptive control system can be relaxed so that the convergent performance of the estimated internal resistance and OCV is enhanced. Particularly, two filters are conceived to mitigate measurement noise as well as disturbance so as to improve the reliability. The simulations and experiments are both performed to demonstrate that the accurate and robust estimations of the internal resistance and OCV can be achieved. Due to the simplicity of the proposed scheme, it can be easily implemented via electronic circuit design or embedded system programming.

References

[1] B.F.W.H. Heyer, US Patent 2,225,051 (1938).
[2] E.P. Finger, E.M. Marwell, US Patent 4,012,681 (1975).
[3] T. Kikuoka, H. Yamamoto, N. Sasaki, K. Wakui, K. Murakami, K. Ohnishi, G. Kawamura, H. Noguchi, F. Ukigaya, US Patent 4,377,787 (1980).
[4] G.R. Seyfang, US Patent 4,949,046 (1988).
[5] C.C. Christianson, R.F. Bourke, US Patent 3,946,299 (1975).
[6] R.L. Eby, US Patent 4,180,770 (1978).
[7] E. Peled, H. Yamin, I. Reshed, D. Kelrich, S. Rozen, US Patent 4,725,784 (1984).
[8] K. Muramatsu, US Patent 4,678,998 (1985).
[9] A.J. Salkind, C. Fennie, P. Singh, T. Atwater, D.E. Reisner, Journal of Power Sources 80 (1999) 293–300.
[10] O. Gerard, J.N. Patillon, F. d'Alche-Buc, Lecture Notes in Computer Science 1327 (1997) 1095–1100.
[11] S. Grewal, D.A. Grant, IEEE International Conference on Telecommunications Energy 484 (2001) 113–120.
[12] G. Plett, Journal of Power Sources 134 (2004) 277–292.
[13] J. Lee, O. Nam, B.H. Cho, Journal of Power Sources 174 (2007) 9–15.
[14] Y.H. Sun, H.L. Jou, J.C. Wu, IEEE International Conference on Power Electronics and Drive Systems (2007) 262–266.
[15] P.E. Pascope, A.H. Anbuky, IEEE Transactions on Power Electronics 19 (6) (2004) 1515–1522.
[16] R.J. Grube, Master's Thesis, Department of Electrical Engineering, Wright State University, 2008.
[17] H. Blanke, O. Bohlen, S. Buller, R.W. De Doncker, B. Fricke, A. Hammouche, D. Linzen, M. Thele, D.U. Saucer, Journal of Power Sources 144 (2005) 418–425.
[18] B. Hariprakash, S.K. Martha, A. Jaikumar, A.K. Shukla, Journal of Power Sources 137 (2004) 128–133.
[19] B.Y. Liaw, R.G. Jungst, G. Nagasubramanian, H.L. Case, D.H. Doughty, Journal of Power Sources 140 (2005) 157–161.
[20] F. Huet, Journal of Power Sources 70 (1998) 59–69.
[21] C.R. Gould, C.M. Bingham, D.A. Stone, P. Bentley, IEEE International Conference on Power Electronics Specialists (2008) 4381–4385.
[22] I. Snihir, W. Rey, E. Verbitskiy, A. Belfadhel-Ayeb, P.H.L. Notten, Journal of Power Sources 159 (2) (2006) 1484–1487.
[23] Y.H. Chiang, W.Y. Sean, IEEE International Conference on Power Electronics and Intelligent Transportation System 1 (2009) 110–115.

[24] D.W. Dennis, V.S. Battaglia, A. Belanger, Journal of Power Sources 110 (2) (2002) 310–320.
[25] J. Newman, K.E. Thomas, H. Hafezi, D.R. Wheeler, Journal of Power Sources 119–121 (2003) 838–843.
[26] L. Benini, G. Castelli, A. macci, E. Macci, M. Poncino, R. Scarsi, IEEE Transactions on VLSI Systems 9 (5) (2001) 630–640.
[27] L. Gao, S. Liu, R.A. Dougal, IEEE Transactions on Components and Packaging Technologies 25 (3) (2002) 495–505.
[28] R.C. Kroeze, P.T. Krein, IEEE International Conference, 2008, pp. 1336–1342.
[29] M. Krstić, I. Kanellakopoulos, P. Kokotović, Nonlinear and Adaptive Control Design, John Wiley & Sons, 1995.
[30] H.K. Khalil, Nonlinear Systems, Prentice Hall, 1996.
[31] K.S. Narendra, A.M. Annaswamy, International Journal of Control 45 (1) (1987) 127–160.
[32] W.Y. Sean, Y.H. Chiang, C.H. Wu, Y.C. Liang, J.C. Ke, S.M. Lo, The 25th International Battery, Hybrid and Fuel Cell Electric Vehicle Symposium & Exhibition, 2010.